# Ultrafast electronic excitations of small sodium clusters and the onset of electron thermalization

**T. Klamroth and M. Nest***

*Received 5th August 2008, Accepted 22nd September 2008*
*First published as an Advance Article on the web 31st October 2008*
**DOI: 10.1039/b813619j**

In this paper we report simulations of the ultrafast laser excitation and relaxation of the correlated valence electrons of a $Na_8$ cluster. The aim is twofold: first, while the total energy stays constant when the exciting laser pulse is over, we observe that the entropy computed from the reduced one electron density matrix rises on a much longer time scale. We discuss whether this can be understood as the onset of the thermalization of a finite system. Second, we describe this process with eight different methods of wavefunction-based electronic structure theory, which have been adapted for an explicitly time-dependent description. Their respective advantages and limitations for the simulation of the excitation and subsequent relaxation are explained.



## I. Introduction

The real-time monitoring of electron motion has recently been achieved experimentally.[1–4] This breakthrough was possible mainly due to the impressive advances in laser technology.[5,6] Consequently, also a largely increased theoretical attention to electron dynamics emerged, compared to the early stages of research[7–9] in the 1980s and early 1990s. Nowadays many theoretical investigations are concerned for instance with the laser-driven electron dynamics in atoms,[10] molecules,[11–19] metal clusters[20] and nanoscale systems.[21]

Nevertheless, it is still a challenging task to obtain an exact solution of the time-dependent electronic Schrödinger equation for systems containing more than a few electrons. A widely used method for an approximate solution is the (explicitly) time-dependent density functional theory[22] (see for instance ref. 20, 23, 24 and 25). Within this method the electron correlation is treated through an approximate exchange–correlation functional. As an alternative, wavefunction-based approaches can be extended beyond the time-dependent Hartree–Fock theory,[7] in order to include electron correlation. The TD-CI (time-dependent configuration interaction)[21,26,27] and MCTDHF (multiconfigurational time-dependent Hartree–Fock)[14,28–30] methods are two examples for time-dependent approaches using multi-determinantal wave functions, in order to treat correlation effects.

A very interesting aspect of correlated many-electron dynamics are electron–electron scattering processes,[31] which are responsible, *e.g.*, for the ultra-short lifetimes of excited electrons in metals or at metal surfaces. These lifetimes are typically of the order of a few femtoseconds (fs). Such very fast electron–electron scattering can lead to a thermalization of the electron gas within about 100 fs,[32] long before any substantial energy transfer to lattice vibrations occurs. However, in many cases these scattering processes cannot be treated explicitly. Instead they are incorporated in kinetic models like the two-temperature model[33] or described in an effective one-electron picture, *e.g.*, by one-electron wave packet propagations with optical potentials,[34] or by relaxation rates for one-electron density matrices[35] and reduced one-electron density matrices.[36]

In the present paper we investigate to what extent we can observe the onset of thermalization after an ultrafast optical excitation in a small system. For this we use a $Na_8$ cluster with eight valence electrons, which are treated explicitly in the quantum dynamical simulations. The methods used are the TD-CIS (time-dependent configuration interaction singles), TD-CIS(D) (single excitations and perturbative treatment of double excitations), TD-CISD (inclusion of single and double excitations), TD-CASCI (inclusion of a truncated complete active space, see below) and MCTDHF methods with different active spaces.

Reduced one-electron density matrices are computed from the many-electron wave functions, in order to evaluate one particle properties during the propagations. Here, we focus on two questions: (i) can we see a delayed process after an ultrafast excitation, which can be regarded as an onset of thermalization in the electronic degrees of freedom? (ii) Is there a suitable one particle operator for the evaluation of one particle energies even for strongly interacting electrons?

The paper is organized as follows. In section II the many-electron dynamics methods used are introduced. In section III the $Na_8$ cluster and its ground-state properties are described. The dynamical simulations and their interpretation are given in section IV. Finally, section V summarizes the paper and gives an outlook for future work. We use atomic units throughout, if not stated otherwise.

## II. Propagation methods for many-electron dynamics

In this section the methods used to solve the time-dependent electronic Schrödinger equation,

$$i\frac{\partial\Psi(\{\vec{x}_i\};t)}{\partial t} = \hat{H}(t)\Psi(\{\vec{x}_i\};t), \qquad (1)$$

are briefly introduced. Here, $\Psi(\{\vec{x}_i\};t)$ is a function of all electron coordinates, $\vec{x}_i$, where $\vec{x}_i = (\vec{r}_i,\omega_i)$ denotes a joint

*Universität Potsdam, Institut für Chemie, Karl-Liebknecht-Str. 24-25, 14476 Potsdam, Germany. E-mail: mnest@uni-potsdam.de*

spatial and spin coordinate. $\hat{H}(t)$ is a time-dependent Hamiltonian, which consists of the time-independent field-free electronic Hamiltonian, $\hat{H}_0$, and the system laser-field interaction. $\hat{H}_0$ is given for a system of $N$ electrons and $N_A$ nuclei with charges $\{Z_A\}$ and positions $\{\vec{R}_A\}$ as

$$\hat{H}_0 = -\frac{1}{2}\sum_i^N \vec{\nabla}^2 + \sum_i^N \sum_{j>i}^N \frac{1}{r_{ij}} - \sum_A^{N_A}\sum_i^N \frac{Z_A}{R_{iA}}, \quad (2)$$

with

$$r_{ij} = |\vec{r}_i - \vec{r}_j|, \quad (3)$$

$$R_{iA} = |\vec{r}_i - \vec{R}_A|. \quad (4)$$

The system-field interaction is treated within the semi-classical dipole approximation

$$\hat{H}(t) = \hat{H}_0 - \vec{\hat{\mu}}\vec{F}(t), \quad (5)$$

where $\vec{\hat{\mu}}$ is the molecular dipole operator

$$\vec{\hat{\mu}} = -\sum_i^N \vec{r}_i + \sum_A^{N_A} Z_A \vec{R}_A. \quad (6)$$

Note that we always work in the fixed nuclei approximation, *i.e.*, all $\vec{R}_A$ are kept constant. This means we focus completely on the electron dynamics, which should be a reasonable approximation for short enough time scales.

The applied laser fields are chosen as $z$-polarized $\sin^2$-shaped pulses, *i.e.*, $\vec{F}(t) = (0,0,F_z(t))^{\mathrm{T}}$, with

$$F_z(t) = F_0 s(t)\sin(\omega t), \quad (7)$$

$$s(t) = \begin{cases} \sin^2(\frac{\omega}{2}t) & 0<t<\frac{2\pi}{\omega} \\ 0 & \text{otherwise} \end{cases}. \quad (8)$$

The frequency of this one-cycle pulse is chosen such that $2\pi/\omega = 1$ fs in all cases. The amplitude, $F_0$, is varied, in order to study the fluence dependence of the laser-driven electron dynamics (see section IV).

The basic ansatz of all many-electron dynamics methods applied in this study is to represent $\Psi(\{\vec{x}_i\};t)$ as a sum of Slater determinants, $\Phi(\{\vec{x}_i\};t)$, *i.e.*, electron configurations, which means anti-symmetrized products of single electron functions, so-called spin orbitals, $\varphi(\vec{x};t)$.

$$\Psi(\{\vec{x}_i\};t) = \sum_j C_j(t)\Phi_j(\{\vec{x}_i\};t) \quad (9)$$

Here, for the TD-CI methods the orbitals and thus the Slater determinants are chosen time-independent, $\Phi_j(\{\vec{x}_i\};t) = \Phi_j(\{\vec{x}_i\})$, leaving only the coefficients, $C_j(t)$, time-dependent. In the MCTDHF ansatz both, the coefficients and the orbitals are time-dependent. Also the various TD-CI and MCTDHF methods differ in which and how many electron configurations $\{\Phi_j\}$ are included in the representation of the many-electron wave function.

### A. TD-CI

The applied TD-CI methods use the same ansatz for the wave function, *i.e.*, the selection of electron configurations, as their time-independent analougs for the calculations of ground and excited electronic states. Therefore, first these time-independent methods are briefly outlined, before the actual propagation methods will be described.

The starting point for all CI methods in this work is the restricted Hartree–Fock (RHF) ground-state Slater determinant, which is obtained by solving the spin-free RHF equations[37]

$$\hat{f}(\vec{r})\psi_i(\vec{r}) = \varepsilon_i\psi_i(\vec{r}). \quad (10)$$

Here, $\hat{f}$ is the Fock operator,

$$\hat{f} = \hat{h}_e + \hat{v}_{HF} \quad (11)$$

which consist of the so-called core-Hamiltonian, $\hat{h}_e = \hat{v}_{\mathrm{ext}} + \hat{t}_e$, describing a single electron in the potential provided by the nuclei, and the HF-potential, $\hat{v}_{HF}$, which contains the Coulomb and exchange interaction between the electrons. The $N/2$ lowest molecular spatial orbitals (MOs), $\psi_i$, are doubly occupied and they form the RHF ground-state configuration, $\Phi_0^{HF}$. All others are unoccupied. Consequently, two orthogonal spin orbitals are constructed from one spatial orbital as

$$\varphi_{\mathrm{j}}(\vec{x}) = \psi_i(\vec{r})\alpha(\omega), \quad \mathrm{j} = 2i - 1, \quad (12)$$

$$\varphi_{\mathrm{k}}(\vec{x}) = \psi_i(\vec{r})\beta(\omega), \quad \mathrm{k} = 2i. \quad (13)$$

In the following spin orbitals will be labeled by non-italic and spatial orbitals by italic indices.

**a CIS.** Within the CIS[38] method, the electronic wave function is written as a linear combination of the HF ground-state Slater determinant and singly excited configurations. These excited determinants are derived from the HF ground state determinant by exciting an $\alpha$ electron from an occupied spatial MO $a$ to an unoccupied spatial MO $r$ ($\Phi_a^r$) or similarly for a $\beta$ electron ($\Phi_{\bar{a}}^{\bar{r}}$). $\Phi_a^r$ and $\Phi_{\bar{a}}^{\bar{r}}$ are combined to so-called singlet configuration state functions (CSFs) in order to form pure singlet spin states (see ref. 37)

$${}^1\Phi_a^r = \frac{1}{\sqrt{2}}(\Phi_{\bar{a}}^{\bar{r}} + \Phi_a^r). \quad (14)$$

The representation of $\hat{H}_0 - E_{HF}$ in this basis yields the CIS Hamiltonian, $\boldsymbol{H}^{CIS}$, where $E_{HF}$ is the RHF ground state energy. Excited state wave functions, $\Psi_i^{CIS}$, and excitation energies, $E_i^{CIS}$, are obtained by diagonalizing $\boldsymbol{H}^{CIS}$

$$\boldsymbol{H}^{CIS}\vec{D}_i = E_i^{CIS}\vec{D}_i \quad (15)$$

$$\Psi_i^{CIS} = D_{0,i}\Phi_0^{HF} + \sum_{a,r} D_{a,i}^r {}^1\Phi_a^r. \quad (16)$$

Here, it is $\Psi_0 = \Phi_0^{HF}$, *i.e.*, the ground state is still given by the RHF wave function, because all Hamiltonian matrix elements $\langle\Phi_0^{HF}|\hat{H}_0 - E_{HF}|{}^1\Phi_a^r\rangle$ are zero.

**b CISD.** In addition, the following doubly excited singlet CSFs[37] are used for the CISD wave function

 

$$^{1}\Psi_{aa}^{rr} = \Psi_{a\bar{a}}^{r\bar{r}},$$

$$^{1}\Psi_{aa}^{rs} = \frac{1}{\sqrt{2}}(\Psi_{a\bar{a}}^{r\bar{s}} + \Psi_{a\bar{a}}^{s\bar{r}}),$$

$$^{1}\Psi_{ab}^{rr} = \frac{1}{\sqrt{2}}(\Psi_{\bar{a}b}^{\bar{r}r} + \Psi_{a\bar{b}}^{r\bar{r}}),$$

$$^{A}\Psi_{ab}^{rs} = \frac{1}{\sqrt{12}}(2\Psi_{ab}^{rs} + 2\Psi_{\bar{a}\bar{b}}^{\bar{r}\bar{s}} - \Psi_{\bar{a}b}^{\bar{s}r} + \Psi_{\bar{a}b}^{\bar{r}s} + \Psi_{a\bar{b}}^{r\bar{s}} - \Psi_{a\bar{b}}^{s\bar{r}}),$$

$$^{B}\Psi_{ab}^{rs} = \frac{1}{2}(\Psi_{\bar{a}b}^{\bar{s}r} + \Psi_{\bar{a}b}^{\bar{r}s} + \Psi_{a\bar{b}}^{r\bar{s}} + \Psi_{a\bar{b}}^{s\bar{r}}).$$

The diagonalization of the corresponding CISD Hamiltonian, $\boldsymbol{H}^{CISD}$, yields the CISD energies and wave functions. Here, the ground-state energy is lower than the RHF ground-state energy, because the doubly excited Slater determinants have non-vanishing Hamiltonian matrix elements with the RHF ground-state wave function.

**c CIS(D).** In the CIS(D) method the doubly excited configurations are included perturbatively,[39,40] *i.e.*, for the results presented here as corrections, $E_i^{(D)}$, to the ground and excited state energies obtained from a CIS calculation:

$$E_i^{CIS(D)} = E_i^{CIS} + E_i^{(D)}. \tag{17}$$

The corrections are calculated from quantities derived from two electron integrals over spin orbitals, $u_{\mathrm{ab},i}^{\mathrm{rs}}$ and $v_{\mathrm{a},i}^{\mathrm{r}}$, spin orbital energy differences, $\Delta_{\mathrm{ab}}^{\mathrm{rs}}$, and the spin orbital coefficients, $D_{\mathrm{a},i}^{\mathrm{r}}$, which are readily obtained through eqn (14) from the CFS coefficients $D_{a,i}^{r}$ (for details see ref. 26 and 39).

$$E_i^{(\mathrm{D})} = -\frac{1}{4}\sum_{\mathrm{abrs}}\frac{(u_{\mathrm{ab},i}^{\mathrm{rs}})^2}{\Delta_{\mathrm{ab}}^{\mathrm{rs}} - E_i^{\mathrm{CIS}}} + \sum_{\mathrm{ar}} D_{\mathrm{a},i}^{\mathrm{r}} v_{\mathrm{a},i}^{\mathrm{r}}. \tag{18}$$

These corrections are derived such that the ground-state energy is identical to the MP2 energy.[37]

**d Truncated CASCI.** For the truncated CASCI the excited electron configurations are created within an certain active space ($N_{act}$,$M$), where $N_{act}$ stands for the number of electrons and $M$ for the number of spatial orbitals within the active space. In the present calculations the active space is comprised of the $N_{act}/2$ highest occupied spatial orbitals and the $M - N_{act}/2$ lowest unoccupied orbitals. Different to a conventional CASCI not all possible excitations within this active space are used, but only those configurations are kept, for which the sum of the indices of spin orbitals forming the configuration is smaller than a certain threshold. In the present study we use a (6,11) active space and a threshold of 70. Again, the electronic Hamiltonian, $\boldsymbol{H}^{CASCI}$, is expressed in the basis of the selected configurations and diagonalized.

**e Time propagation.** In order to solve eqn (1), the wave function is expanded in the basis of the corresponding CI eigenstates

$$\Psi(t) = \sum_i C_i(t)\Psi_i. \tag{19}$$

The initial wave function at $t = 0$ is chosen to be the ground-state wave function of the respective CI method. During the interaction with the laser field, the wave function is propagated using an operator splitting technique (see ref. 41 and references therein)

$$\vec{C}(t + \Delta t) = \boldsymbol{U}_z^{\dagger} e^{iF_z(t)\tilde{\boldsymbol{\mu}}_z\Delta t}\boldsymbol{U}_z e^{-i\tilde{\boldsymbol{H}}\Delta t}\vec{C}(t). \tag{20}$$

$\tilde{\boldsymbol{H}}$ is the diagonal Hamilton matrix in CI eigenstate basis. $\boldsymbol{U}_z$ is a unitary matrix which transforms from the CI eigenstate basis to a basis in which the dipole matrix $\tilde{\boldsymbol{\mu}}_z$ is diagonal. $\Delta t$ was chosen as 0.5 attoseconds (as) for all TD-CI method except TD-CASCI where $\Delta t = 10$ as was used. At times, where the laser pulse is already off, $t \geq t_f = \frac{2\pi}{\omega}$, the propagation becomes trivial.

$$\Psi(t_f + \Delta t) = \sum_i C_i(t_f)\exp(-iE_i^{\mathrm{CI}}\Delta t)\Psi_i \tag{21}$$

## B. MCTDHF

In MCTDHF the time-dependent wave function is not only expanded in many configurations with time-dependent coefficients, but also the MOs forming these configurations are time-dependent:

$$\begin{aligned}\Psi(\{\vec{x}_i\};t) &= \sum_J^{\mathrm{ord}} C_J(t)\Phi_J(\{x_i\};t) \\ &= \sum_J^{\mathrm{ord}} C_J(t)|\varphi_{\mathrm{j}_1}(\vec{x}_1;t)\ldots\varphi_{\mathrm{j}_N}(\vec{x}_N;t)|.\end{aligned} \tag{22}$$

Capital $J$ is a composite index, consisting of $N$ small $\mathrm{j}_i$, which enumerate the $N$ spin orbitals in an electron configuration. The summation is performed only over ordered $J$ to ensure independent electron configurations. Here, all possible configurations for a given number of spin orbitals, $n = 2M$, and active electrons, $N_{act}$, are used, *i.e.*, $\binom{n}{N_{act}}$. As for CASCI, we use the common CASSCF notation ($N_{act}$,$M$) for a system with an active space of $N_{act}$ electrons and $M$ spatial orbitals, which are used to form the spin orbitals. The equations of motion for the time-dependent coefficients, $C_J(t)$, and the orbitals are obtained from the Dirac–Frenkel variational principle:

$$\frac{\mathrm{d}}{\mathrm{d}t}C_J = -i\sum_L\langle\Phi_J(\{x_i\};t)|\hat{H}|\Phi_L(\{x_i\};t)\rangle C_L, \tag{23}$$

$$\frac{\partial}{\partial t}\varphi_{\mathrm{j}} = -i\sum_{\mathrm{kl}}(1-P)_{\mathrm{jk}}\left(h_{\mathrm{kl}} + \sum_{\mathrm{m}}\rho_{\mathrm{km}}^{-1}\langle V_{ee}\rangle_{\mathrm{ml}}\right)\varphi_{\mathrm{l}}. \tag{24}$$

Here, $P$ is a projector on the space spanned by the single particle functions

$$\hat{P} = \sum_{\mathrm{j}=1}^{n}|\varphi_{\mathrm{j}}\rangle\langle\varphi_{\mathrm{j}}|. \tag{25}$$

$h_{\mathrm{kl}}$ is an element of the core Hamiltonian matrix in spin orbital representation, which contains the single electron kinetic energy and the electron–nuclei attraction. $\rho_{\mathrm{km}}^{-1}$ and $\langle V_{ee}\rangle_{\mathrm{ml}}$ are matrix elements of the reduced one electron density matrix

and the mean field matrix $\langle V_{ee}\rangle$, where $V_{ee}$ describes the Coulomb repulsion between the electrons (for further details see ref. 29 and 30). The equations of motion above are integrated using an adaptive step size Runge–Kutta integrator of order eight.

### C. One-electron properties

We compute one-electron properties from the time-dependent wave function through the reduced one electron density matrix $\rho_{ij}$, which is represented in the basis of the RHF ground state orbitals

$$\rho_{ij}(t) = \langle\varphi_i|\hat{\rho}|\phi_j\rangle. \quad (26)$$

Here, $\hat{\rho}$ is computed from the time-dependent many-electron wave function as

$$\rho(\vec{x}',\vec{x};t) = N\int\Psi(\vec{x}',\ldots,\vec{x}_N;t)^{\star}\Psi(\vec{x},\ldots,\vec{x}_N;t)d\vec{x}_2\ldots d\vec{x}_N. \quad (27)$$

The diagonal elements, $\rho_{ii}$, are the populations in the HF-ground state orbitals and are used to estimate the Fermi energy and temperature of the system (see section IV).

## III. Model system: the $Na_8$ cluster

The geometry of the used $Na_8$ cluster is displayed in Fig. 1. It was obtained by a geometry optimization at the HF level of theory using the CEP-4G basis set (which will be denoted small basis set in the following) together with the corresponding effective core potential[42] within the Gaussian03 program package.[43] The geometry optimization started from a broken symmetry octahedron with one additional Na-atom in the center of the octahedron and another one above one face of the octahedron. The overall structure is close to a tetrahedron with edges roughly 7.5 Å long. Additional calculations where performed with a split basis set (termed big basis set) and a comparable effective core potential,[44] *i.e.*, which also leaves eight electrons in total in the calculations.

The ground-state energy and the ground-state permanent dipole moment are given in Table 1 for both basis sets and various methods. The Hartree–Fock ground-state energy is −1.422871 $E_h$ (1 $E_h$ = 1 Hartree = 27.211 eV) for the small basis set. CASCI(6,11), MP2/CIS(D) and CISD yield ground state correlation energies of about −0.030, −0.060 and −0.075 $E_h$ for this basis set. The MCTDHF methods systematically recovers more correlation energy when more unoccupied orbitals are included in the active space, *i.e.*, the correlation is −0.006 for MCTDHF(8,5) and reaches −0.032 $E_h$ for MCTDHF(8,7). All methods predict a nearly vanishing permanent dipole moment for the chosen $Na_8$ cluster. As shown in Table 1, we get comparable results for the big basis set, *e.g.*, correlation energies of roughly −0.073 $E_h$ and −0.089 $E_h$ for MP2/CIS(D) and CISD. Therefore, we focus in section IV exclusively on time-dependent results obtained with the small basis, as calculation with all methods are feasible with this basis set. Also the basis-set dependence of the dynamical results is very small, as exemplified in the second last paragraph of section IV.

**Fig. 1** Optimized geometry for the $Na_8$ cluster. Calculations were done at the RHF/CEP-4G level of theory. For details see text.

**Table 1** Ground-state energies and permanent dipole moments of the cluster for (a) the small and (b) the big basis set. Energies are given in $E_h$ and dipole moments in $ea_0$. Note, the dipole moment for CIS(D) is the RHF one, as in the present study only perturbative corrections to the energies are calculated

| | $E_0$ | $\mu_x$ | $\mu_y$ | $\mu_z$ |
|---|---|---|---|---|
| (a) | | | | |
| CIS/RHF | −1.422871 | −0.0952 | −0.0587 | 0.0200 |
| CIS(D) | −1.482991 | — | — | — |
| CISD | −1.498667 | −0.0604 | −0.0372 | 0.0125 |
| CASCI(6,11) | −1.453135 | −0.230 | 0.0699 | 0.0942 |
| MCTDHF(8,5) | −1.429165 | 0.0541 | 0.0347 | −0.0119 |
| MCTDHF(8,6) | −1.440773 | −0.0519 | −0.0288 | −0.113 |
| MCTDHF(8,7) | −1.454413 | −0.169 | −0.103 | 0.0363 |
| (b) | | | | |
| CIS/RHF | −1.462754 | −0.173 | −0.106 | 0.0366 |
| CIS(D)/MP2 | −1.535699 | — | — | — |
| CISD | −1.551335 | −0.209 | −0.128 | 0.0439 |

## IV. Results

In order to illustrate the basic effect that is the subject of this paper, we start by comparing the time evolution of the total energy and the entropy of the eight valence electrons, after laser excitation. The laser pulse is a Fourier limited 1 fs/1 cycle pulse, with an energy per photon of 0.151982 $E_h$, corresponding to a wave length of 300 nm.

Fig. 2 shows the response of the sodium cluster to a laser pulse with 10.28 GV $m^{-1}$, calculated with MCTDHF(8,6). The upper panel contains the energy expectation value. During the 1 fs of the pulse, the electrons absorb about 0.1 $E_h$, and when the pulse is over, the energy stays constant. This is in contrast to the evolution of the entropy of the system, shown in the lower panel. We calculated this property according to

$$S = -\mathrm{Tr}\{\rho\ \ln(\rho)\}, \quad (28)$$

*i.e.*, without the Boltzmann prefactor, and with a normalization such that the trace of the one-electron density matrix is equal to the number of electrons, as is common in electronic structure theory. This normalization has also the advantage, that the entropy of the Hartree–Fock ground state, where each spin orbital has an occupation number of one, is zero. Fig. 2 shows clearly that there is relaxation dynamics going on, on a time scale of several femtoseconds, after the laser pulse is over. The origin of the difference of time-scales between the two panels is obviously, that the upper panel shows an $N$-electron property, while the lower panel gives information derived from a single particle picture. The general trend of the entropy is to



 

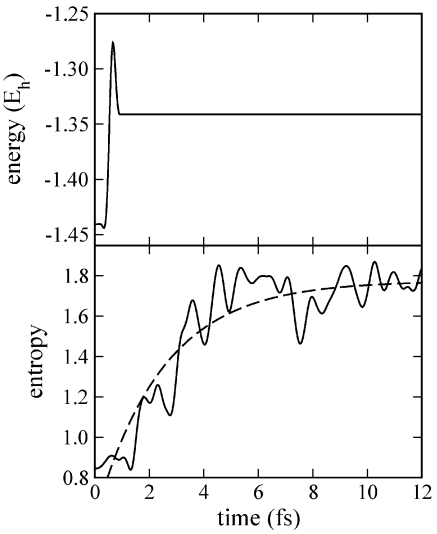


**Fig. 2** Energy and entropy production in the system of the 8 valence electrons of the $Na_8$ cluster. While the energy stays constant after the 1 fs/1 cycle pulse, the entropy continues to increase over a time scale of several fs, signaling relaxation in the single particle picture. The calculation was done at the MCTDHF(8,6) level of theory, and a maximum field strength of 10.28 GV $m^{-1}$. The dashed line in the lower panel is a monoexponential fit.

increase, a hallmark of thermalization. In how far this term is really justified will be discussed later. On top of the increase of the entropy, oscillations are visible, which stem from the fact that we are dealing with a finite size system.

In order to discuss thermalization, we have to evaluate whether the single particle states are occupied according to the Fermi–Dirac (FD) distribution. For this purpose we calculated the populations of the Hartree–Fock ground state orbitals before and after the excitation. From the TD-CI calculations this quantity is immediately available, in the case of MCTDHF we project the time-dependent orbitals onto the HF orbitals. While the HF populations are uniquely defined for the ground state, it is somewhat more difficult to determine them for times when the laser pulse is over. The reason for this is that the pulse creates a superposition of eigenstates, so that the HF orbital populations become oscillatory. In order to extract 'final' occupation numbers nevertheless, we performed a time-average for the time interval from 10 fs to 30 fs, well after the relaxation process is over. Fig. 3 shows the initial (circles) and final (squares) HF populations for the same field strength of 10.28 GV $m^{-1}$ and method, MCTDHF(8,6), that were used in Fig. 2. Also shown are least-square fitted Fermi–Dirac distributions. The first thing to note is that even the ground state has a finite temperature of about 6760 K. This is because we are dealing with a *correlated* ground state, to which excited determinants, in the CI picture, also contribute. For nuclear degrees of freedom a temperature of 6760 K would be huge, but compared to electronic energy scales this is quite moderate. However, it is clear that the notion of a temperature of a correlated system has to be taken with a grain of salt. We will come back to this point later. After the laser pulse and the relaxation process are over, we find a temperature of 13 150 K. The agreement between populations and fit is not excellent, but still qualitatively correct.

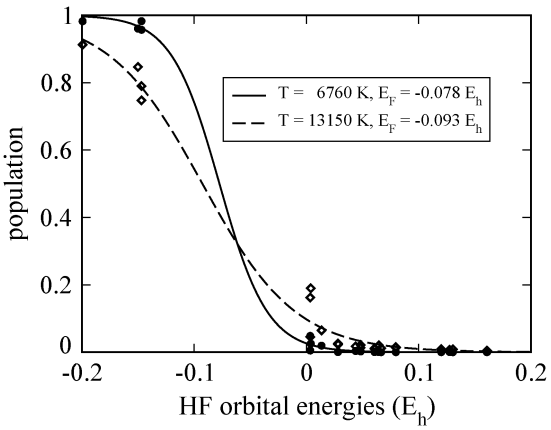


**Fig. 3** Initial and final populations of Hartree–Fock spin orbitals, and fit to FD distributions. Calculation at the MCTDHF(8,6) level of theory, and a maximum field strength of 10.28 GV $m^{-1}$.

Quantitatively the difference can be expressed by the root-mean-square (rms) deviation. For the final distribution in Fig. 3 the rms deviation is 0.0276. This is a typical value, as can be seen from Table 2, which compares the final state rms deviations of the fitted temperatures, for all methods and field strengths used in this study. There are a few trends that can be extracted from this table. One is that CI-based methods generally have a lower rms deviation than methods with time-dependent orbitals. The origin of this is probably the nonlinear nature of the equations of motion of MCTDHF, which inserts some degree of noise into the results. A second conclusion is, that higher correlated methods produce generally higher rms deviations. We will address this question of convergence later in this paper.

Before we continue, it is necessary to discuss whether the choice of Hartree–Fock populations and orbital energies for the temperature fitting of Fig. 3 can be justified, and whether there are other single particle pictures, which are more reasonable. This choice of single particle picture is equivalent to asking: what kind of particle is actually thermalizing? If the single particle states are the eigenfunctions of the Fock operator, then we are dealing with quasiparticles. One can ask in the same way, how the 'physical' electrons behave. In this case one has to project on the eigenfunctions of the single

**Table 2** The rms deviation of final Hartree–Fock populations from a Fermi–Dirac distribution. The final distribution in Fig. 3 (MCTDHF(8,6), field strength 10.28 GV $m^{-1}$) has a rms deviation of 0.0276, which is in the middle of the range. Generally, higher field strengths result in higher rms deviations, and CI methods have lower rms deviations than MCTDHF

| | Field strength | | | |
|---|---|---|---|---|
| Method | 1.29 GV $m^{-1}$ | 2.57 GV $m^{-1}$ | 5.14 GV $m^{-1}$ | 10.28 GV $m^{-1}$ |
| CIS | 0.0009 | 0.0032 | 0.0092 | 0.0166 |
| CIS(D) | 0.0009 | 0.0028 | 0.0085 | 0.0154 |
| CISD | 0.0062 | 0.0064 | 0.0072 | 0.0141 |
| CASCI(6,11) | 0.0028 | 0.0032 | 0.0065 | 0.0260 |
| TDHF | 0.0005 | 0.0019 | 0.0067 | 0.0189 |
| (8,5) | 0.0077 | 0.0085 | 0.0269 | 0.0161 |
| (8,6) | 0.0097 | 0.0099 | 0.0643 | 0.0276 |
| (8,7) | 0.0074 | 0.0170 | 0.0486 | 0.0463 |

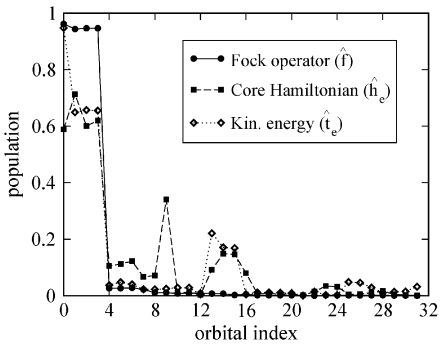


**Fig. 4** Single-electron state populations, for Hartree–Fock electrons (quasiparticles), 'physical' electrons, and a free-electron gas, derived from the correlated CISD ground state.

electron Hamiltonian, *i.e.*, the core Hamiltonian $\hat{h}_e$. Or one could argue, that the valence electrons of a possibly metallic $Na_8$ cluster form a free-electron gas. The question here is whether eight electrons are enough to form a conduction band with non-interacting Bloch electrons. In this case one needs to project on eigenfunctions of the single electron kinetic energy operator $\hat{t}_e$. Fig. 4 compares the populations for the three cases, and the correlated CISD ground state. Obviously, only the Hartree–Fock populations are similar to a FD distribution. In both other cases, the 'physical' electrons and the free-electron gas, the single particle picture breaks down, because the interactions, and thus the correlations are too strong. Also, the qualitatively good agreement of the Hartree–Fock result with a FD distribution indicates that the sodium cluster is still quite close to a molecule.

The more energy is absorbed by the cluster, the higher the temperature will be in the end. Therefore, the question to address now is: by how much does the energy rise during the laser pulse, and how is this related to the field strength/fluence and the used method? Fig. 5 shows our results for the energy uptake, $\Delta E(F_0)$. It can be seen that at most one photon is absorbed. The first thing to note is, that an ultrashort pulse is not sensitive to the exact positions of the excited-state energies, because it is very broad in energy. Therefore, the results are remarkably similar. Second, we find a saturation effect for TD-CIS and TD-CIS(D): They are leveling off at higher fluences, because doubly excited determinants would become more important. The fact, that TD-CISD is consistently above all other methods, while there is only a small difference if one goes from TDHF to MCTDHF(8,7) is rather surprising. It might be explained by the observation, that the latter method accounts for only 0.86 eV of correlation energy, while TD-CISD accounts for 2.1 eV. Obviously, even MCTDHF(8,7) is still far from convergence quantitatively, at least as far as the energy uptake is concerned. A qualitative result that is reproduced by all methods is the super-linear scaling of $\Delta E(F_0)$. Though no common exponent exists, it is an interesting finding, when compared to the fluence dependence of the temperature, to be discussed next.

Fig. 6 shows the results of the least-square temperature fitting for all eight methods and the same range of laser field strengths as above. Again, the upper panel contains the CI based methods, and the lower panel the TD orbital based

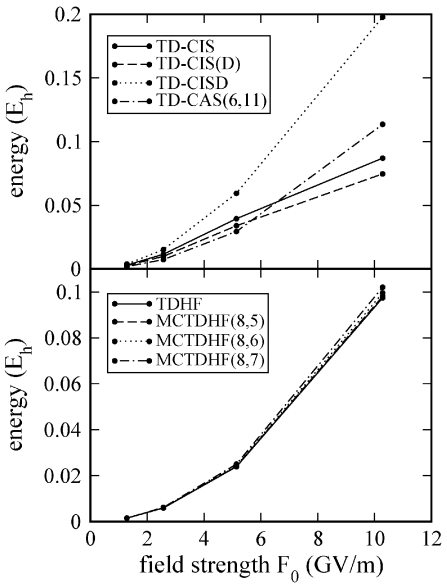


**Fig. 5** Energy uptake as a function of maximum field strength, $F_0$.

methods. TD-CIS and TD-CIS(D) produce almost identical temperatures, just as for the energy. However, there is now a large gap to TD-CISD and TD-CASCI, because the latter start from a correlated ground state, and thus from a finite temperature larger than zero. The good agreement between TD-CISD and TD-CASCI at low field strengths indicates that these calculations are close to convergence. The rather high temperature from TD-CASCI at field strength 10.28 GV $m^{-1}$ is most likely a saturation effect due to the limited number of 11 spatial orbitals. The picture is more complicated for the (MC)TDHF calculations. An increase of active space clearly changes the results. It is difficult to assess whether the MCTDHF(8,7) result is at least near convergence, but its good agreement with TD-CISD and TD-CASCI is promising.

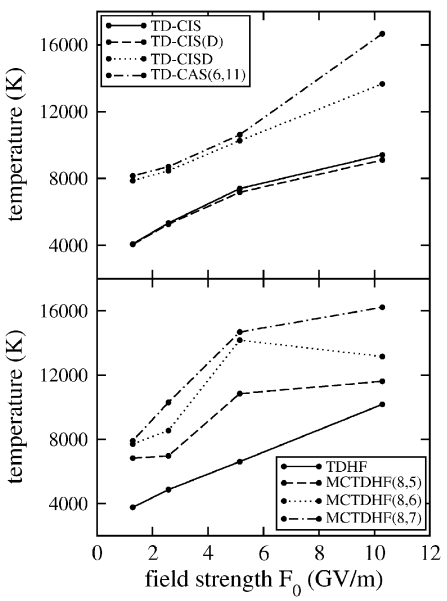


**Fig. 6** Least-square fitted temperatures to Hartree–Fock spin orbital populations, as a function of maximum field strength.

 

The unusual, high temperatures at 5.14 GV m$^{-1}$ coincide with large rms deviations, indicating that the ordinate values of these points are not very reliable (see Table 2). A functional form for the dependence of the final temperature on the field strength can not be derived easily. However, the function $T(F_0)$ is closer to being linear than the function $\Delta E(F_0)$, impliying a rise of the heat capacity with temperature, as expected.

Let us now come back to the entropy of the system, and the process of relaxation. According to Fermi-liquid theory, the lifetime $\tau_i$ of an excited single particle level $\varepsilon_i > \varepsilon_F$ decreases according to

$$\tau_i \propto \frac{1}{(\varepsilon_i - \varepsilon_F)^2}. \qquad (29)$$

Therefore, we expect an increase in the relaxation rate, with increasing field strength, *i.e.*, energy uptake. In order to estimate this rate, we fitted a mono-exponential function of the form

$$S(t) = A - B\exp(-\gamma t) \qquad (30)$$

to the TD entropy, see the dashed line in Fig. 2. We are aware that the exact dynamics is multi-exponential, but the noisy nature of the entropy does not permit the extraction of more detailed information. Fig. 7 shows the rates $\gamma$ defined by eqn (30), for three selected methods, and the usual range of field strengths. Both CI methods reproduce the expected increase of the rate, whereas MCTDHF does not show a clear trend. There are two reasons for this difference. The first reason has to do with the size of the one-electron reduced density matrix. For (MC)TDHF kind of methods, the size is equal to the number $n$ of spin orbitals squared. Any density matrix of a given size has a certain maximum entropy that can be represented, given by $-N\ln(N/n)$ in our normalization. In other words, in the case of TDHF the entropy is a constant of the motion, $S(t) = S_{max} = 0$, for (8,5) the maximum entropy is 1.8, for (8,6) $S_{max} = 3.2$, and for (8,7) one finds $S_{max} = 4.5$. Compared to CASCI(6,11), where $S_{max} = 8.1$ and CISD, where $S_{max} = 16.6$, the entropy production is clearly limited for (MC)TDHF.

A second effect is illustrated in Fig. 8. For the field strength of 5.14 GV m$^{-1}$ the evolution of the entropy is shown for three different methods. In the case of TD-CIS (upper panel), the entropy does not change after the laser pulse is over. The restriction to only singly excited determinants suppresses scattering events, which lead to a net transfer of population from occupied to unoccupied orbitals, *i.e.*, the total population within in the unoccupied MO is fixed after the laser pulse is off. TD-CISD (middle panel), takes significantly more correlation into account, so that such scattering events can be described. The same is true for MCTDHF (lower panel). As this method corresponds to the CASSCF method of time-independent quantum chemistry, multiple excitations are accounted for, and the time-dependent orbitals can be linear combinations of arbitrary HF orbitals. However, the time-dependence of the orbitals also introduces an artificial time-dependence into the density matrix, making the entropy much more oscillatory. Also, while the entropy changes by about 1.5 in the case of TD-CISD, it changes by only 0.3 in the case of MCTDHF(8,6), because the 6 spatial orbitals can form only a rather small reduced density matrix.

In this context the question arises of how much these results depend on the basis set used to represent the orbitals. The small basis set used for the calculation above contains four basis functions per electron, and could thus probably be seen as insufficient. Therefore, we compared some of our results with calculations performed with the big basis set, see section 3. We found, that the results for both sets are almost the same. Exemplarily we show in Fig. 9 the time-dependent entropy from TD-CISD, and for a maximum field strength of 5.14 GV m$^{-1}$. They agree very well, except for minor details of the oscillations.

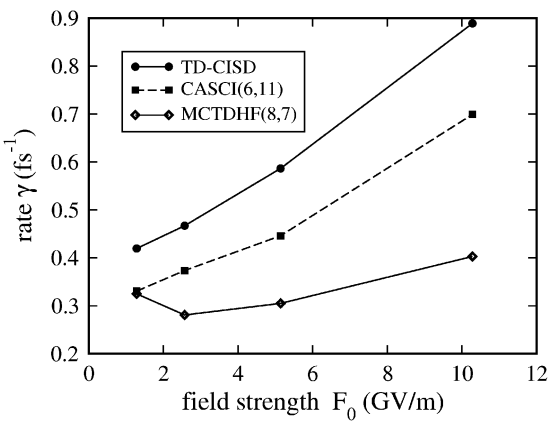


**Fig. 7** Relaxation rates as a function of field strength, $F_0$, and thus of energy uptake, deduced from the time-dependent entropy, by fitting a mono-exponential function, see eqn (30). While the CI-based methods reproduce the expected increase of the rate in accordance with Fermi-liquid theory, MCTDHF does not show this trend. For discussion, see text.

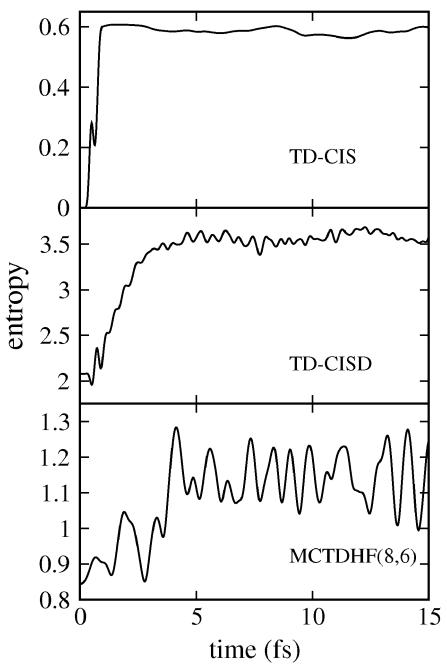


**Fig. 8** Comparison of entropy production/relaxation for three different methods, and a maximum field strength of 5.14 GV m$^{-1}$.

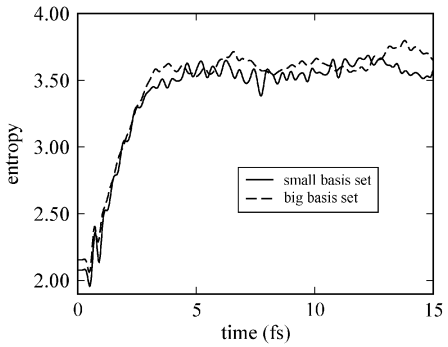


**Fig. 9** Comparison of the entropy, calculated for the two different basis sets, and a maximum field strength of 5.14 GV $m^{-1}$ within the TD-CISD method. The good agreement indicates that the small basis set is large enough.

That process, that has been tentatively called thermalization up to now, can also be looked at from a different perspective. The laser pulse excites a superposition of several eigenstates of the *N*-electron Hamiltonian, and here especially those with a large transition dipole moment, which are traditionally identified with plasmons.[25,45–48] However, there is little agreement on questions like the degree of anharmonicity and the number of eigenstates that contribute to a plasmon peak. Some of the discrepancies can probably be attributed to the fact, that the approximation of jellium potentials have been made. On the other hand it is interesting to note, that it was experimentally found that plasmons in sodium clusters decay on a time scale of about 10 fs,[49] due to anharmonicity in the potential of even a single excitation. In light of this, the rise of the entropy (Fig. 2 and 8) can probably also be identified with the decay of a plasmon: a superposition of *N*-electron eigenstates implies (in general) a non-stationary population of single-particle basis functions, which is reflected in the entropy. This ultrashort time scale has to be distinguished from the much slower process of thermalization involving electron–phonon coupling (or electron-vibration coupling, in the case of a cluster). In this paper we discussed only the first, ultrafast process, which also justifies the fixed-nuclei approximation.

## V. Summary

In this paper we presented calculations of the correlated dynamics of the eight valence electrons in a $Na_8$ cluster. The focus was on an *ab initio* description of the relaxation dynamics, following an ultrashort, and therefore spectrally broad, laser pulse. Even though the system is isolated/closed after the pulse is over, we find that the dynamics in the single particle picture continues for several femtoseconds. This is especially clearly seen in the rise of the entropy, which can be interpreted as the onset of thermalization, or the decay of a plasmon. This phenomenon requires, that a superposition of electronic eigenstates is populated by the laser pulse, which has therefore to be spectrally broad. The details of the pulse, like polarization or exact wave length are not important.

Furthermore, we showed that the populations of the Hartree–Fock orbitals are close to a Fermi–Dirac distribution even after excitation, while the single particle picture of 'physical' electrons and a free electron gas is not appropriate here.

Additionally, we compared eight different wave function based methods of electronic structure theory, which were adapted to an explicitly time-dependent description. While all methods were able to describe energy-related quantities quite well, we found that for quantum statistical properties a sufficiently large reduced density matrix is required. Those methods, like TD-CISD, which support a large reduced density matrix, give qualitatively good results also for the temperature-dependent heat capacity and the energy-dependent relaxation rates.

## Acknowledgements

MN gratefully acknowledges support through grant SPP 1145 of the Deutsche Forschungsgemeinschaft.

## References

1 M. Hentschel, R. Kienberger, C. Spielmann, G. A. Reider, N. Milosevic, T. Brabec, P. Corkum, U. Heinzmann, M. Drescher and F. Krausz, *Nature*, 2001, **414**, 509.
2 R. Kienberger, M. Hentschel, M. Uiberacker, C. Spielmann, M. Kitzler, A. Scrinzi, M. Wieland, T. Westerwalbesloh, U. Kleineberg, U. Heinzmann, M. Drescher and F. Krausz, *Science*, 2002, **297**, 1144.
3 P. Bucksbaum, *Nature*, 2003, **421**, 593.
4 A. Föhlisch, P. Feulner, F. Hennies, A. Fink, D. Menzel, D. Sanchez-Portal, P. Echenique and W. Wurth, *Nature*, 2005, **436**, 7049.
5 G. G. Paulus, F. Lindner, H. Walther, A. Baltuška, E. Goulielmakis, M. Lezius and F. Krausz, *Phys. Rev. Lett.*, 2003, **91**, 253004.
6 X. Liu, H. Rottke, E. Eremina, W. Sandner, E. Goulielmakis, K. O. Keeffe, M. Lezius, F. Krausz, F. Lindner, M. G. Schätzel, G. G. Paulus and H. Walther, *Phys. Rev. Lett.*, 2004, **93**, 263001.
7 K. C. Kulander, *Phys. Rev. A*, 1987, **36**, 2726.
8 R. Grobe and J. H. Eberly, *Phys. Rev. A*, 1993, **48**, 4664.
9 M. S. Pindzola, P. Gavras and T. W. Gorczyca, *Phys. Rev. A*, 1995, **51**, 3999.
10 S. Laulan and H. Bachau, *Phys. Rev. A*, 2003, **68**, 013409.
11 H. Yu and A. D. Bandrauk, *Phys. Rev. A*, 1997, **56**, 685.
12 F. Remacle and R. Levine, *J. Chem. Phys.*, 1999, **110**, 5089.
13 K. Harumiya, H. Kono, Y. Fujimura, I. Kawata and A. D. Bandrauk, *Phys. Rev. A*, 2002, **66**, 043403.
14 T. Kato and H. Kono, *Chem. Phys. Lett.*, 2004, **392**, 533.
15 X. Chu and S.-I. Chu, *Phys. Rev. A*, 2004, **70**, 061402.
16 G. Paramonov, *Chem. Phys. Lett.*, 2005, **411**, 350.
17 T. Burnus, M. Marques and E. Gross, *Phys. Rev. A*, 2005, **71**, 010501.
18 I. Barth and J. Manz, *Angew. Chem. Intern. Ed.*, 2006, **45**, 2962.
19 I. Barth, J. Manz, Y. Shigeta and K. Yagi, *J. Am. Chem. Soc.*, 2006, **128**, 7043.
20 F. Calvayrac, P.-G. Reinhard, E. Suraud and C. A. Ullrich, *Phys. Rep.*, 2000, **337**, 493.
21 T. Klamroth, *Phys. Rev. B*, 2003, **68**, 245421.
22 E. Runge and E. K. U. Gross, *Phys. Rev. Lett.*, 1984, **52**, 997.
23 T. Kunert and R. Schmidt, *Eur. Phys. J. D*, 2003, **25**, 15.
24 E. Livshits and R. Baer, *Journal of Physical Chemistry A*, 2006, **110**, 8443.
25 Y. Kurzweil and R. Baer, *Phys. Rev. B*, 2006, **73**, 075413.
26 P. Krause, T. Klamroth and P. Saalfrank, *J. Chem. Phys.*, 2005, **123**, 074105.
27 P. Krause, T. Klamroth and P. Saalfrank, *J. Chem. Phys.*, 2007, **127**, 034107.
28 F. Zanghellini, M. Kitzler, C. Fabian, T. Brabec and A. Scrinzi, *Laser Physics*, 2003, **13**, 1064.
29 M. Nest, T. Klamroth and P. Saalfrank, *J. Chem. Phys.*, 2005, **122**, 124102.

30 M. Nest, P. Ramanathan and P. Saalfrank, *J. Chem. Phys.*, 2007, **126**, 214106.
31 M. Nest and T. Klamroth, *Phys. Rev. A*, 2005, **72**, 012710.
32 M. Bonn, D. N. Denzler, S. Funk, M. Wolf, S.-S. Wellershoff and J. Hohlfeld, *Phys. Rev. B*, 2000, **61**, 1101.
33 S. I. Anisimov, B. L. Kapeliovich and T. L. Perel'man, *Sov. Phys. JETP*, 1974, **39**, 375.
34 J. Sjakste, A. G. Borisov and J. P. Gauyacq, *Nucl. Instr. and Meth. in Phys. B*, 2003, **203**, 49.
35 T. Klamroth, P. Saalfrank and U. Höfer, *Phys. Rev. B*, 2001, **64**, 035420.
36 N. Buecking, M. Scheffler, P. Kratzer and A. Knorr, *Appl. Phys. A*, 2007, **88**, 505.
37 A. Szabo and N. S. Ostlund, *Modern Quantum Chemistry*, McGraw-Hill, New York, first (revised) edn, 1989.
38 J. B. Foresman, M. Head-Gordon, J. A. Pople and M. J. Frisch, *J. Phys. Chem.*, 1992, **96**, 135.
39 M. Head-Gordon, R. J. Rico, M. Oumi and T. J. Lee, *Chem. Phys. Lett*, 1994, **219**, 21.
40 M. Head-Gordon, D. Maurice and M. Oumi, *Chem. Phys. Lett.*, 1995, **246**, 114.
41 A. D. Bandrauk, E. Aubanel and S. Chelkowski, in *Femtosecond Chemistry*, ed. J. Manz and L. Wöste, Verlag Chemie, Weinheim, Germany, 1995, vol. 2, chap. 25, p. 731.
42 W. Stevens, H. Basch and J. Krauss, *J. Chem. Phys.*, 1984, **81**, 6026.
43 M. J. Frisch, G. W. Trucks, H. B. Schlegel, G. E. Scuseria, M. A. Robb, J. R. Cheeseman, J. A. Montgomery, Jr., T. Vreven, K. N. Kudin, J. C. Burant, J. M. Millam, S. S. Iyengar, J. Tomasi, V. Barone, B. Mennucci, M. Cossi, G. Scalmani, N. Rega, G. A. Petersson, H. Nakatsuji, M. Hada, M. Ehara, K. Toyota, R. Fukuda, J. Hasegawa, M. Ishida, T. Nakajima, Y. Honda, O. Kitao, H. Nakai, M. Klene, X. Li, J. E. Knox, H. P. Hratchian, J. B. Cross, V. Bakken, C. Adamo, J. Jaramillo, R. Gomperts, R. E. Stratmann, O. Yazyev, A. J. Austin, R. Cammi, C. Pomelli, J. Ochterski, P. Y. Ayala, K. Morokuma, G. A. Voth, P. Salvador, J. J. Dannenberg, V. G. Zakrzewski, S. Dapprich, A. D. Daniels, M. C. Strain, O. Farkas, D. K. Malick, A. D. Rabuck, K. Raghavachari, J. B. Foresman, J. V. Ortiz, Q. Cui, A. G. Baboul, S. Clifford, J. Cioslowski, B. B. Stefanov, G. Liu, A. Liashenko, P. Piskorz, I. Komaromi, R. L. Martin, D. J. Fox, T. Keith, M. A. Al-Laham, C. Y. Peng, A. Nanayakkara, M. Challacombe, P. M. W. Gill, B. G. Johnson, W. Chen, M. W. Wong, C. Gonzalez and J. A. Pople, *GAUSSIAN 03 (Revision C.02)*, Gaussian, Inc., Wallingford, CT, 2004.
44 P. J. Hay and W. R. Wadt, *J. Chem. Phys.*, 1985, **82**, 284.
45 V. Kresin, *Phys. Rep.*, 1992, **220**, 1.
46 M. Koskinen, M. Manninen and P. Lipas, *Phys. Rev. B*, 1994, **49**, 8418.
47 F. Catara, P. Chomaz and N. V. Giai, *Phys. Rev. B*, 1994, **48**, 18207.
48 F. Catara, D. Gambacurta, M. Grasso and M. Sambataro, *Phys. Lett. A*, 2006, **349**, 345.
49 R. Schlipper, R. Kusche, B. von Issendorff and H. Haberland, *Phys. Rev. Lett.*, 1998, **80**, 1194.